pp 660–679. © Royal Aeronautical Society 2017
doi: 10.1017/aer.2017.10

Investigation of self-deploying high-lift effectors applied to membrane wings

N. Osterberg
Oregon State University
Mechanical, Industrial, and Manufacturing Engineering
Corvallis
USA

R. Albertani
roberto.albertani@oregonstate.edu
Oregon State University
Mechanical, Industrial, and Manufacturing Engineering
Corvallis
USA

ABSTRACT

Flow separation followed by aerodynamic stall limits the operation of aircraft. Expanding the flight envelope of aircraft has been a goal of aerodynamicists for decades. This work presents findings from tests in the Oregon State University wind tunnel investigating the effectiveness of a passively actuated suction-surface flap on membrane wings. Experiments were conducted on a rigid plate and membrane wings with and without a pop-up flap. All wings had an aspect ratio of 2, while membrane pre-strain and Reynolds number were varied. An increase in lift at stall was observed for all testing conditions with flap deployment. The observed average increase in maximum lift varied from 5% to 15% for different test conditions. The variation in flap effectiveness is compared to membrane pre-strain, Reynolds number, and wing camber. A quadratic relationship between modelled camber and flap effectiveness is observed, and an optimal level of membrane camber is found to maximise flap effectiveness.

Keywords: Membrane aerofoil; pliant wing; pop-up flap; feather flap; high-lift effector

Received 12 April 2016; revised 12 December 2016; accepted 13 December 2016; first published online 30 March 2017.

NOMENCLATURE

AR	aspect ratio
b	span, $[m]$
c	chord, $[m]$
C_L	coefficient of lift
C_D	coefficient of drag
C_M	coefficient of moment about $\frac{1}{4}$ chord
DIC	digital image correlation
E	Young's modulus, $[GPa]$
MAV	micro aerial vehicle
Re	Reynolds number
S	planform area, $[m^2]$
t	membrane thickness, $[mm]$
U	flow velocity, $[m/s]$
We	Weber number
Z	maximum out of plane membrane deflection
Z^*	Z / c
θ	flap deployment angle, [Degrees]
λ_o	membrane pre-stretch
ν	kinematic viscosity of air, $[m^2/s]$
π_2	aeroelastic parameter for membrane stiffness
ρ	density of air, $[Kg/m^3]$
σ	membrane spanwise stress, $[MPa]$

1.0 INTRODUCTION

Aerodynamic stall limits the operation of aircraft. Finding methods to expand the flight envelope of aircraft has been a goal of aerodynamicists and aircraft designers for decades. As a result, there are many forms of high-lift devices used to delay the onset of stall. Observation of natural flyers has been a source of inspiration for aerodynamics since before the beginning of human flight[1]. Nearly 60 years before the Wright Brothers' first flight, F.H. Wenham published a paper in which he observed that the relative speed at which birds flew appeared to be related to the ratio of span to chord of their wings. This is the origin of Aspect Ratio (AR)[2]. Studies investigating the flight of animals continue today. Recent studies of flapping flight show potential to improve the performance of Micro Air Vehicles (MAVs)[3,4] – an unmanned aircraft having a maximum dimension of 15 cm and operating at speeds of below 15 m/s. The feasibility of such vehicles was first proposed by RAND Corporation[5] before a formal definition by the U.S. Defense Advanced Research Projects Agency (DARPA)[6].

1.1 Background Information – High-Lift Effectors

One type of high-lift device inspired by natural flyers is the suction-surface pop-up flap. Many types of birds have feathers on the top surface of their wings, from the greater secondary coverts and marginal coverts feather groups[7], which deploy as separated flow develops from the wing's trailing edge and delay aerodynamic stall. Figure 1 shows a duck and a raven, both with pop-up flap deployed during landing. This behaviour of bird wings has been mimicked in various experiments with a flap attached to the top surface of a wing[8-13]. The flap is hinged

https://doi.org/10.1017/aer.2017.10 Published online by Cambridge University Press

Figure 1. (Colour online) A mallard (left) and a raven (right) as they flare for landing. Notice the feathers that are standing up on the top of the wing close to the wing root.

about its leading edge and the trailing edge of the flap is left free. During the transition to a regime of fully separated flow, a region of flow reversal develops on the aft portion of the top surface of the wing; this reversed flow lifts the flap. The flap rotates until the weight of the flap and the force from the normal flow on the raised edge of the flap are in equilibrium with the force from the reversed flow pushing on the inner aft portion of the flap[14]. The lifted flap provides a physical barrier to delay the forward propagation of separated flow over the suction surface of the wing, delays the onset of stall, and increases the angle-of-attack for maximum lift.

The first known observation of this effect was by W. Liebe, who hypothesised that the feathers that popped up during high angle-of-attack flight were a biological high-lift device. His observations inspired a research project in 1938 where a leather flap was affixed to one wing of a Messerschmitt 109 to quantify the effect. The presence of the flap on one wing of the aircraft resulted in compromised aerodynamic stability and inconclusive results[14]. The effect of the passive flap was successfully quantified in 1996 at the German Aerospace Center (DLR) with a similar experiment to the Messerschmitt 109, but utilising a passive flap attached to each wing of a glider with an HQ-41 aerofoil. The flap was found to produce a 7% increase in coefficient of lift (C_L) at stall[12,15]. In the years since 1997, many researchers have advanced our understanding of the pop-up flap in many areas including: optimisation of flap size and position[12,14,16-18], optimisation of flap material and geometry[9,17,19], flap deployment angle[10,19-22], flap performance at low Reynolds Number (Re)[11], using pop-up flaps for drag reduction[23], dynamic testing with the pop-up flap[24], testing of pop-up flaps on highly elliptical low AR wings[25], kinematics and stability of the wing and flap[26-28], the effects of having multiple flaps[18], and how hairy surfaces can have a similar function to the pop-up flap[8,29].

1.2 Background Information – Membrane Wings

Another form of bio-mimicry in aerodynamics is the utilisation of membrane wings. As technology has advanced to allow for the creation of MAVs, aircraft stability at low Re has become increasingly important. As the size of an aircraft is reduced, the aircraft's inertia scales more quickly than the aerodynamic forces, resulting in increased susceptibility to perturbation from gusty environmental conditions[30,31]. Bats and sugar gliders are two examples of natural flyers that utilise membrane wings and fly with agility in conditions similar to those where

https://doi.org/10.1017/aer.2017.10 Published online by Cambridge University Press

current MAVs struggle to achieve flight stability. Membrane wings are flexible and deflect with increasing aerodynamic loads or Re; as the load is increased, the membrane camber is enhanced. One method of adjusting the camber is membrane pre-strain or excess length[32-34]. Research has been conducted on the aerodynamics of membrane wings[32,35-38]. The benefits of membrane wings have inspired many MAV designers to emulate natural flyers[39-41]. The use of membrane wings has been shown to increase maximum lift as compared to its rigid wing counterpart[42]. Such wings have been experimentally found to increase small aircrafts' gust tolerance[43,44] and aerodynamic damping[45]. The deformed shapes of membrane wings are also significantly sensitive to their edge constraints. The form of gust tolerance cited by Abudaramv is specific to membrane wings with a free trailing edge[43], which are fundamentally different in the way they passively change wing twist with aerodynamic loading than the perimeter supported membranes investigated in this work. Due to the benefits of both membrane wings and pop-up flaps, there is interest in the interactions of membrane wings and the pop-up flap.

1.3 Research Objectives

The objectives of this project were to

1. Investigate if the pop-up flap remains effective when applied to pliant wings.
2. Determine if membrane pre-strain and Re have a significant impact on the effectiveness of the pop-up flap.
3. Determine if membrane camber has a significant effect on flap effectiveness.

2.0 WIND TUNNEL AND TESTING APPARATUS

The experiments were conducted in the closed-loop low-speed (up to 18 m/s) wind tunnel at Oregon State University (OSU). The tunnel test section is 1.52 m wide and 1.22 m high by 9.14 m long. Turbulence level is less than 0.3% and solid blockage factor with the wing investigated in this paper is 34.15×10^{-6}. The angle-of-attack of the wing was changed by rotating a u-shaped arm, shown in Fig. 2. This arm was attached to a rotational servo motor through the wall of the wind tunnel; this allowed for the angle-of-attack to be driven remotely.

The sting balance used in this experiment was a three-forces, three-moments sensor with full scale loads of 13.35 N for normal force, 8.897 N for side and axial force, 0.5650 N.m for pitch moment and 0.3390 N.m for roll and yaw moment. Two standard deviation accuracies on full-scale loads are 0.11% for normal, 0.09% for axial and 0.12% for side forces, 0.15% for pitch, 0.16% for roll and 0.11% for yaw moments, respectively[46].

2.1 Data Acquisition

An analogue-to-digital converter (National Instruments CompactRio) was utilised to capture all six channels of data from the sting balance, along with the air temperature, airspeed, angle-of-attack and airspeed control voltage. A LabVIEW Visual Interface (VI) then ran a PID controller to adjust the angle-of-attack and airspeed, sent updated control voltages back to the analogue-to-digital converter, and exported aerodynamic loads data to a text file. This text file was later used for more advanced data processing using R-Studio and MATLAB.

https://doi.org/10.1017/aer.2017.10 Published online by Cambridge University Press

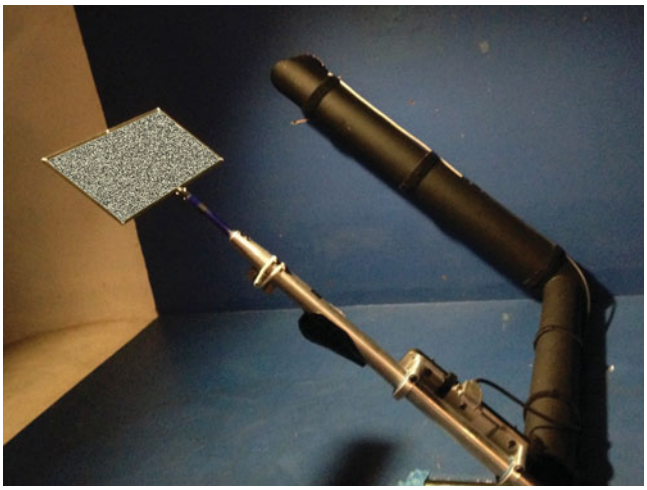

Figure 2. (Colour online) The variable angle-of-attack apparatus that supports the test article in the wind tunnel.

2.2 Test Article

The reference rigid wing consisted of a flat plate with the same chord and wingspan as the membrane wing, ellipsoidal leading edge and trailing edge and a thickness of 3.1 mm.

The membrane wing test article had an aspect ratio of 2, as shown in Fig. 3. This wing was constructed from two steel frames, with a chord of 140 mm and a span of 280 mm, which sandwich the membrane from the top and bottom. The frames were bonded to the pre-strained membrane.

In order to stretch the membrane to the desired level of pre-strain, a speckled sheet of latex rubber was placed onto the membrane pre-strain fixture in its fully retracted state (139.7 mm by 381 mm), shown in Fig. 4. This fixture allows for each edge of the membrane to be pulled independently by tightening one of four screws. Two cameras, mounted above the pre-strain fixture, were used to capture images of the slack membrane. The membrane was stretched, and another set of images was recorded. Both sets of images were used for Digital Image Correlation (DIC) in VIC3D in order to determine the state of strain of the membrane[47,48].

The stretching process resulted in the measured average membrane strain in both the spanwise direction (y-axis) and the chordwise direction (x-axis) at the desired level of pre-strain to within 0.5%. The rigid frame was then adhered to the middle portion of the membrane while still in place on the pre-strain fixture using a spray adhesive applied to the one side of the frame (this allowed for avoiding the corners of the membrane where the strain is measured to be the least consistent). After the adhesive had set, the membrane was removed from the pre-strain fixture, the other side of the aerodynamic frame was adhered to the backside of the membrane, and the excess material was trimmed from the wing's edges. Once the pre-strained membrane was attached to the steel frame, the wing was mounted at its trailing edge to the sting balance.

The pop-up flap was constructed from a piece of 110lb card stock (0.22 mm thickness), and had a chord of 0.2 c. The flap was attached to the wing at a position of 0.6 c from the leading edge with a 1 cm wide strip of Scotch Tape 3710 polypropylene film (with an average thickness of 0.048 mm, tensile strength of 771.0 N/100 mm of width and Young's modulus

https://doi.org/10.1017/aer.2017.10 Published online by Cambridge University Press

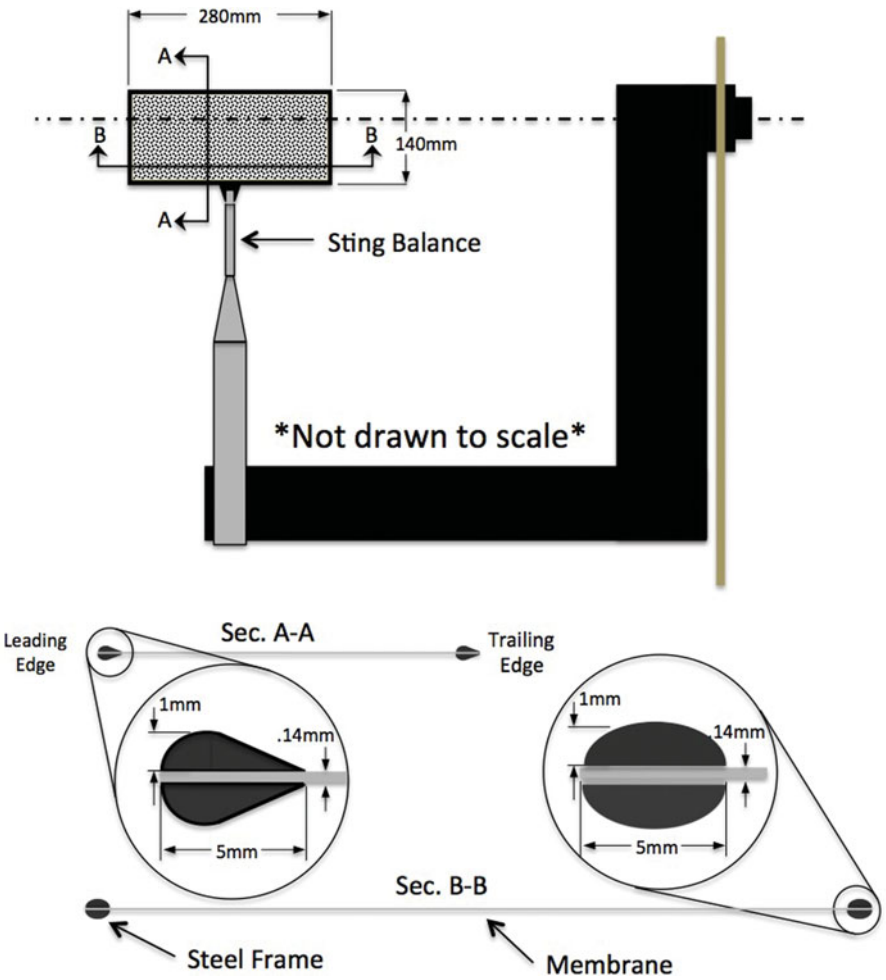

Figure 3. (Colour online) The geometry of the frame that supports the membrane wing.

of 1,300-1,800 MPa, according to the manufacturer's technical data sheet). The flap size and position were based on published experimental results for a rigid wing[11,20,21]. To avoid the flap from being mechanically bound by the coupling of its stiffness and the spanwise deflection of the membrane on which the flap is hinged, the flap was cut along its spanwise direction into five sections free to rotate about their hinge. The centre flap is $\frac{1}{3}b$ in span while the flaps closer to the wing tips are each $\frac{1}{6}b$ in span (see Fig. 5). The flaps do not constrain the wing membrane in the chordwise direction and minimally constrain the membrane in the spanwise direction on the hinge line.

3.0 EXPERIMENTAL FACTORS

An elastic membrane wing and a rigid flat-plate were tested with and without the pop-up flap for three different Re. Each test condition was repeated three times. Twelve hundred data points were recorded at a sampling frequency of 500 Hz at each angle-of-attack tested, and the

https://doi.org/10.1017/aer.2017.10 Published online by Cambridge University Press

Figure 4. (Colour online) The pre-strain fixture used for adjusting membrane tension.

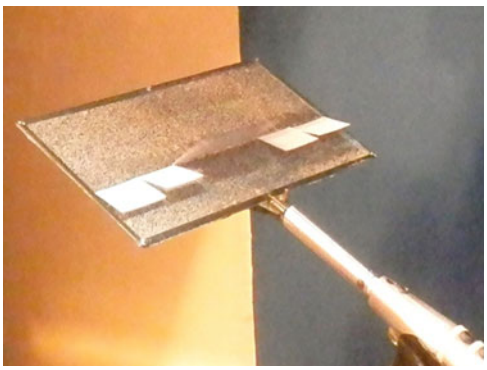

Figure 5. (Colour online) The membrane wing with the attached flap deployed in flow.

LabView program that was used for data collection applied a band stop filter from 58 to 62 Hz to reduce the noise in the data from AC contamination of the signal. All conditions tested are shown in Table 1.

4.0 METHODS

A script was used to collect data between replications. The data for each repetition of each angle-of-attack were reported as a mean and a standard deviation. The mean value of each condition was analysed in the ANOVA. The standard deviations of the means from the three repetitions for each test condition are represented in the error bars on the various figures that follow.

R-Studio was used to conduct a two-way Analysis of Variance test (ANOVA) on each trial to determine the flap's level of significance on the C_L while isolating this effect from that of the angle-of-attack. An independent means model of angle-of-attack and flap condition was created. The ANOVA was then conducted on the angle-of-attack and the flap condition. In the ANOVA, the variation in the model is attributed to the different factors based on the mean squared residuals. Residuals that can not be attributed to one of the factors are a measure of

https://doi.org/10.1017/aer.2017.10 Published online by Cambridge University Press

Table 1
Levels tested for each experimental factor

Experimental Factors	Levels Tested
Wing Configurations	Rigid flat plate
	Pre-strain = 0.075
	Pre-strain = 0.05
	Pre-strain = 0.025
	Slack membrane
Reynolds Number	Re = 50,000
	Re = 75,000
	Re = 83,000
Angle-of-Attack	0° to 28°
Flap Conditions	Clean Wing
	0.2c chord length flap at position 0.6c
Repetitions	3

the error in the ANOVA. The residuals are also tested for normality and equal variance to verify that the fundamental assumptions of the ANOVA are satisfied.

For this experiment, it was anticipated that there may be a relationship between flap effectiveness and wing camber. A metric for membrane camber was needed. Both π_2 and Z^* were used to quantify membrane deformation. π_2, shown in Equation (1)[32], is the aeroelastic stiffness coefficient. This parameter is defined by the ratio of membrane stress, calculated from strain multiplied by the modulus (1.2e6Pa was used as the modulus and is the 100% modulus shown in the data for a similar latex membrane tested by Stanford in 2008[49]), multiplied by membrane thickness over dynamic pressure multiplied by chord, and has an inverse correlation with flow-induced membrane deformation[50].

$$\pi_2 = \frac{\sigma t}{qc} \quad \ldots (1)$$

The modified Waldman 2013 camber model has been previously observed to correlate closely with DIC measurements of camber[51], and is utilised in this paper for the prediction of camber. This model is similar to the model published in Song's 2008 publication[52] and assumes that the membrane deforms to a circular arc, and relates the camber of the membrane to the pressure gradient between the lower and upper surfaces of the wing and the membrane stiffness (Equations (3) and (4). This method correlates the Weber number (Equation (2)) to Z^* membrane displacement nondimensionalised by the wing chord[51]

$$We = \frac{L}{Etb} \quad \ldots (2)$$

In this equation, L is the lift, E is membrane Young's modulus, t is membrane thickness and b is wingspan. From Waldman[51], Equation (3) can be used to estimate Z^* for a given Weber

https://doi.org/10.1017/aer.2017.10 Published online by Cambridge University Press

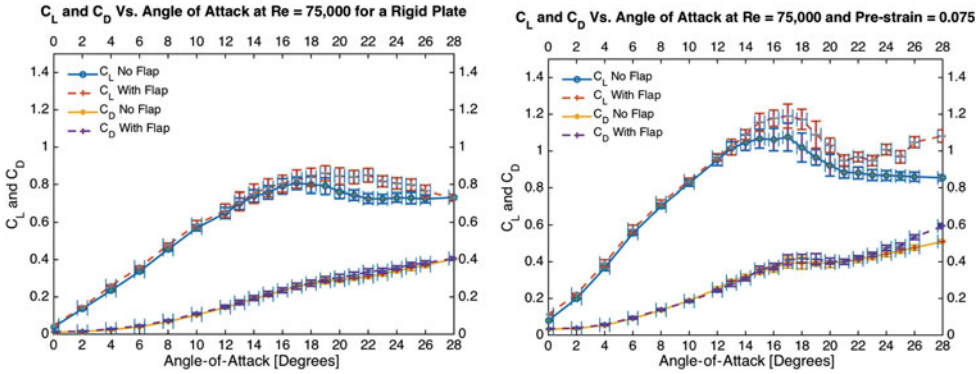

Figure 6. (Colour online) Comparison between the rigid flat plate (left) and a membrane pre-strained to 0.075 (right). Both the lift and drag behaviour is shown for wings with and without flaps, for a Re of 75,000.

number.

$$We \approx 8(\lambda_o - 1)Z^* + \left(\left(\frac{64}{3}\right) - 32\lambda_o - 1\right) Z^{*3} \quad \ldots (3)$$

Finite span change in lift slope (Equation (4)) from Waldman[51] is used to correct the second term of Equation (3).

$$\frac{\delta C_L}{\delta \alpha} = \frac{2\pi}{\frac{2}{AR} + \sqrt{1 + (\frac{2}{AR})^2}} \quad \ldots (4)$$

In order to utilise this model, the Weber number (Equation (2)) was calculated for each test condition. The Weber number was then used with the known value of pre-strain in Equation (3) with the correction from Equation (4) multiplying the second term of Equation (3) to find Z^*, the chord-normalised maximum camber.

Two AOS S-PRI cameras (capable of capturing 1,000 frames per second at 1280×1024 resolution) were mounted above the test article with a stereoscopic angle of approximately 40°. These cameras were utilised to collect synchronised images during each test. Roughly 50 images were captured at a frequency of 100 Hz during each angle-of-attack that was tested.

5.0 RESULTS AND DISCUSSION

Figure 6 shows a comparison of the effect of the pop-up flap on a flat-plate and on the membrane wing with a pre-strain of 0.075. The membrane has a higher increase in the lift force at stall, and has a larger increase in the lift force after stall.

Previous work on pliant membrane wings[39,41,45,47-49,53] shows a correlation between an increasing coefficient of lift and a decrease of pre-strain, for similar test conditions. This correlation is due to the relative increase of camber of the membrane wing when decreasing the membrane pre-strain. For membrane wings, an increase in angle-of-attack below the stall angle causes an increase in lift and camber. This effect is greater in low pre-strain membranes relative to high pre-strain membranes.

https://doi.org/10.1017/aer.2017.10 Published online by Cambridge University Press

5.1 ANOVA

Due to the nature of membrane wings, many modes of vibration are present in the membrane during testing[54]. These vibrations are largely responsible for the variance in the data, which is similar to the variance presented in Waszak's 2001 publication[53]. A two-way ANOVA was conducted on the data from each test condition (across repetitions and angles of attack) to verify that statistical significance was maintained despite experimental noise. The resulting p-values are a measure of the significance of the effects of both the flap and the angle-of-attack. No significant effect of the flap was observed for the rigid plate at a Re of 50,000 or for the slack membrane at a Re of 83,000. All other trials were found to have a p-value of less than 5.0×10^{-5}, which is well below the minimum significance level of 0.05[55]. The *P*-value gives the likelihood of a type 1 error – erroneously rejecting the null hypothesis (that there is no significant effect), when in fact there is no effect. This means that the lower the *P*-value the higher the certainty that the observed effect is significant. The ANOVA table for the first trial of the Re = 75,000 pre-strain = 0.075 test condition is shown in Table 2 as an example.

Table 2
ANOVA table for the Re = 75,000 pre-strain = 0.075 test condition

ANOVA Table

	Df	Sum Sq	Mean Sq	F Stat	*P*-value
Flap	1	0.16609	0.16610	97.126	1.15E-14
Angle-of-Attack	21	7.06994	0.33666	196.867	< 2.2E-16
Residuals	67	0.11458	0.00171		

ANOVA was selected as the statistical metric in this experiment because it is robust to non-normality in data for large sample sizes and robust to non-equal variance of samples if sample sizes are both similar across trials[56], both conditions of which are met by our data. Despite the data analysed making this test robust to violation of the fundamental ANOVA assumptions, normality, equal variance and independence were all still evaluated. Figure 7 shows the normality of the data evaluated for one of the conditions tested.

From the distribution of the residuals for the trial shown in Fig. 7 (left), there is clearly a degree of non-normality in the distribution of the data. From the QQ-plot shown in Fig. 7 (right), it can be observed that the values toward the far right of the chart are not on the theoretical line, indicating a slight lack of normality in the data.

Figure 8 shows the residuals plotted against the fitted values. This chart provides a way to evaluate the equal variance assumption of the ANOVA test. Figure 8 shows that the residuals do not have equal variance, but that they are not so far from constant as to raise concern about the validity of the ANOVA.

5.2 Effect on Lift

Figures 9, 10 and 11 show different test conditions grouped by Re. Each figure is accompanied by a table displaying the *P*-values calculated with the two-way ANOVA for each trial. In each of these plots, each line is the result of three trials, to show a mean accompanied by an error bar representing one standard deviation in the data at each plotted point.

The same data that was presented in Figs 9, 10, and 11 is shown in a different form in Fig. 12, illustrating a direct comparison between the high and low pre-strain conditions and the

https://doi.org/10.1017/aer.2017.10 Published online by Cambridge University Press

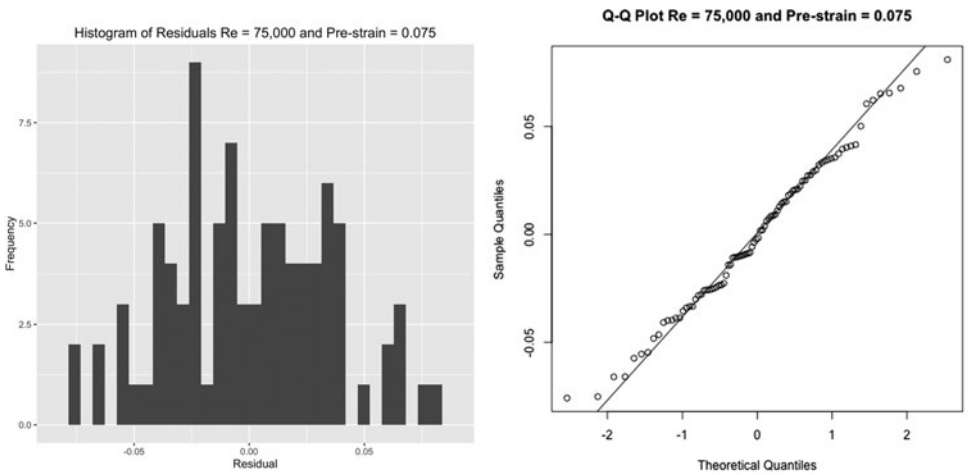

Figure 7. Verification of the normality assumption of the Re = 75,000 pre-strain = 0.075 test condition. The residuals distribution is on the left and the normal probability plot (QQ-plot) of the residuals is on the right.

rigid plate condition with the same flap configuration and Re. It is observed that the measured increase in maximum C_L with the addition of the pop-up flap is greater for the membrane wing than for the equivalent rigid plate case.

It is observed that for many of the membrane test conditions, the C_L curve does not pass through the [0,0]. As such, it is critical to quantify the level of error in the angle-of-attack measurement. The error between the assigned angle-of-attack and the angle-of-attack measured through DIC was evaluated for these three tests. The average errors between assigned angle-of-attack and measured angle-of-attack were 0.302°, 0.364° and 0.212° with standard deviations of 0.227°, 0.198° and 0.055°. This level of error alone is not enough to explain the asymmetry in the C_L vs angle-of-attack graphs. So DIC data was used to evaluate the camber of the membrane wing at 0° angle-of-attack. The evaluation of a subset of DIC data shows that in the low pre-strain tests, there is a significant camber at 0° angle-of-attack. It is suspected that this is due to the asymmetries of the aerodynamic frame causing a pressure gradient and inducing a small camber.

For each of the Re tested, the largest observed increase in C_L at stall is observed for the two higher values of pre-strain (pre-strain = 0.05 and pre-strain = 0.075). An optimum pre-strain is observed in these test conditions between 0.05 and 0.075. Membrane pre-strain and Re were evaluated independently for their influence on flap effectiveness. However, only poor correlations with high residual errors were produced through independent linear regression. The significance of these factors was only revealed when the interaction term of pre-strain and Re was also considered in a two-way ANOVA. By accounting for the interaction term as an additional factor, far more of the variance could be attributed to one of the factors rather than remaining as residual error, increasing the statistical power of the ANOVA. The results of this ANOVA show that the dominant factor in modelling the increase in maximum C_L is the interaction between Re and pre-strain. The individual effects of Re and pre-strain on increase in maximum C_L are also statistically significant.

https://doi.org/10.1017/aer.2017.10 Published online by Cambridge University Press

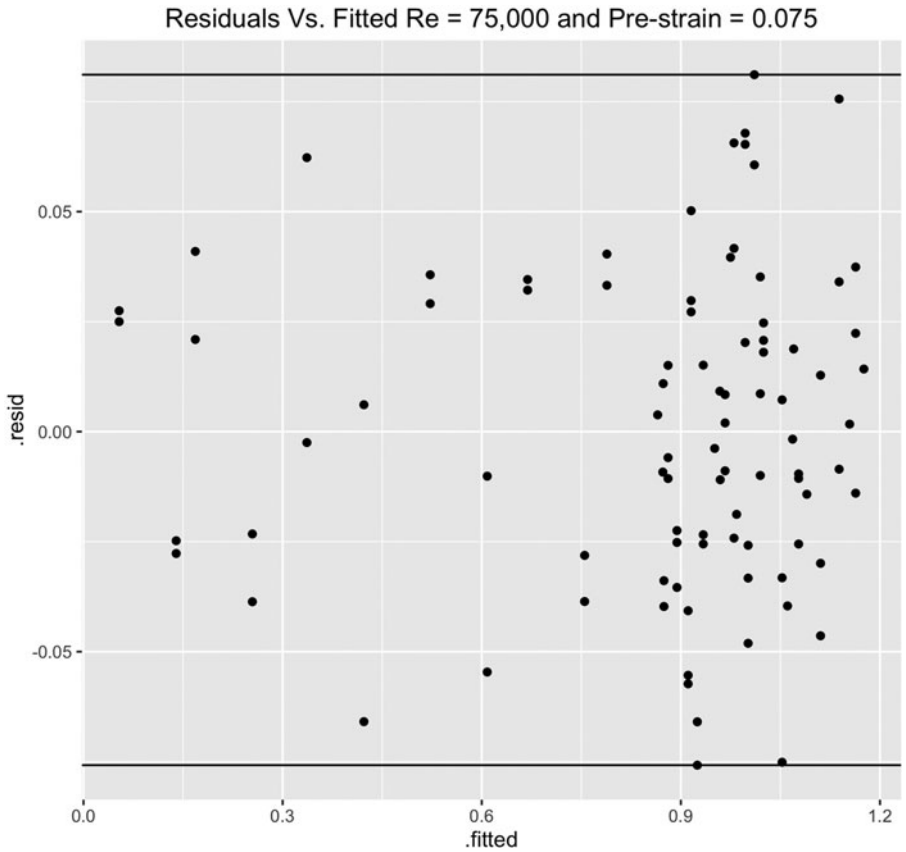

Figure 8. Verification of the assumption equal variance.

5.3 Effect of Camber on Lift

The results of the ANOVA are best understood when one considers that both of these parameters affect the camber of the pliant wing. The more membrane pre-strain, the stiffer the wing and the less camber is observed. Increasing the Re increases the pressure gradient across the membrane, camber and lift. Figure 13 shows the increase in maximum lift with the addition of the flap for each test condition of the membrane wing plotted against π_2. The equation for this parameter, shown in Equation (1), combines both the membrane pre-strain and the free-stream flow velocity (proportional to Re) into one value.

Figure 14 shows the relationship between predicted non-dimensional camber Z^* and the increase in maximum C_L. This is theoretically inversely proportional to the π_2 parameter; however, this parameter does not assume a value of zero for a pre-strain of zero and allows for comparison of the slack membrane trials without the use of an additional parameter. The relationship between increase in maximum C_L and Z^* is fit to a quadratic expression, shown as the regression line in Fig. 14. A region of the membrane of roughly 0.1c immediately ahead of the flap was reinforced by the flap attachment. It is therefore assumed that the membrane has a slightly higher effective modulus when the flap is attached, and that the Z^* will over-predict camber for these conditions. This assumption was checked using DIC data from one

https://doi.org/10.1017/aer.2017.10 Published online by Cambridge University Press

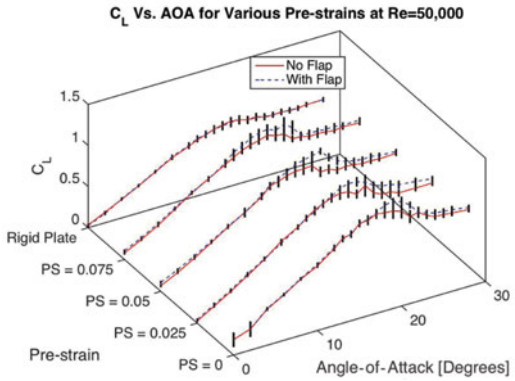

Table 3
***P*-value for the effect of the flap for each test at Re = 50,000**

Pre-strain	Flap p-value
0	1.13E-4
0.025	3.83E-9
0.05	3.00E-11
0.075	8.31E-11
Rigid	0.789

Figure 9. (Colour online) Each test condition for Re = 50,000

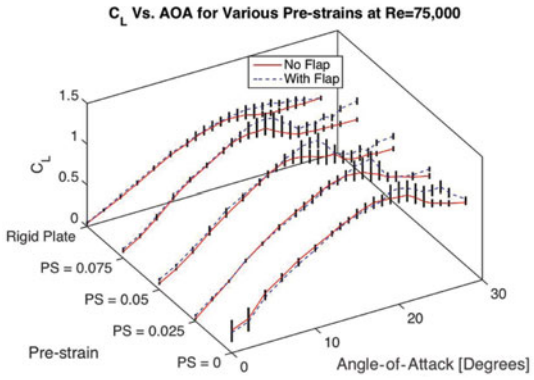

Table 4
The *P*-value for the effect of the flap is reported for each test at Re = 75,000

Pre-strain	Flap *P*-value
0	2.59E-2
0.025	2.87E-3
0.05	1.26E-12
0.075	1.15E-14
Rigid	1.73E-12

Figure 10. (Colour online) Each test condition for Re = 75,000

of the test conditions and it was found that while the membrane displacements were similar, the flapped wing did have a lower measured camber for an equivalent lift force; as such, the *x*-axis of Fig. 14 is predicted camber of the clean wing.

In both Figs 13 and 14, there are two test conditions that do not seem to follow the same trend. The two conditions where the data lies substantially below the quadratic fit are the pre-strain of zero and the pre-strain of 0.025, both at the Re of 50,000 condition. In both of these conditions, the flap deployment was observed to be lesser than most trials, as can be seen in Table 6. The flap loses effectiveness when it folds forward and assumes a flap deployment angle of greater than 90°. In both conditions that do not appear to follow the same trend, the flap never reached a state where it folded forward, so it is likely the flap never reached its optimal deployment angle during these tests conditions.

The implication of the quadratic relationship shown in Fig. 14 is that, for this particular case of flap design and position, there is an optimum level of camber for the performance of the pop-up flap for membrane aerofoils. This result matches the findings of Schlüter, who showed that rigid wings with various aerofoil sections performed differently with the flap[11].

https://doi.org/10.1017/aer.2017.10 Published online by Cambridge University Press

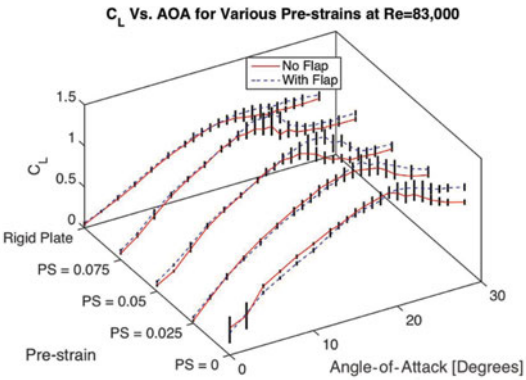

Table 5
The *P*-value for the effect of the flap is reported for each test at Re = 83,000

Pre-strain	Flap *P*-value
0	0.169
0.025	2.96E-3
0.05	3.23E-11
0.075	1.66E-13
Rigid	1.04E-14

Figure 11. (Colour online) Each test condition for Re = 83,000

Table 6
Maximum flap deployment angle observed for each test condition where DIC data was collected

Re	Pre-strain	Maximum flap deployment angle
50,000	Plate	$\theta < 45^\circ$
75,000	Plate	$45^\circ < \theta < 90^\circ$
100,000	Plate	$45^\circ < \theta < 90^\circ$
50,000	0	$45^\circ < \theta < 90^\circ$
75,000	0	$\theta > 135^\circ$
83,000	0	$\theta > 135^\circ$
50,000	0.025	$45^\circ < \theta < 90^\circ$
75,000	0.025	$\theta > 135^\circ$
83,000	0.025	$\theta > 135^\circ$
50,000	0.05	$45^\circ < \theta < 90^\circ$
75,000	0.05	$\theta > 135^\circ$
83,000	0.05	$\theta > 135^\circ$
50,000	0.075	$45^\circ < \theta < 90^\circ$
75,000	0.075	$90^\circ < \theta < 135^\circ$
83,000	0.075	$\theta > 135^\circ$

5.4 Relative Flap Deployment

In the photos collected for DIC of the membrane, it is possible to approximate the angular deflection of the pop-up flap. The maximum observed flap deployment angle is reported in Table 6 for each of the test conditions. Flap angle is 90° when perpendicular to the wing chord.

5.5 Effect on Drag and Pitching Moment

The behaviour of the wing with respect to coefficient of drag (C_D) and coefficient of pitching moment about $\frac{1}{4}$ chord (C_M) is also altered with the addition of the flap. Figure 15 shows the angle-of-attack versus C_D plot (left) and the angle-of-attack versus C_M (right) for the

https://doi.org/10.1017/aer.2017.10 Published online by Cambridge University Press

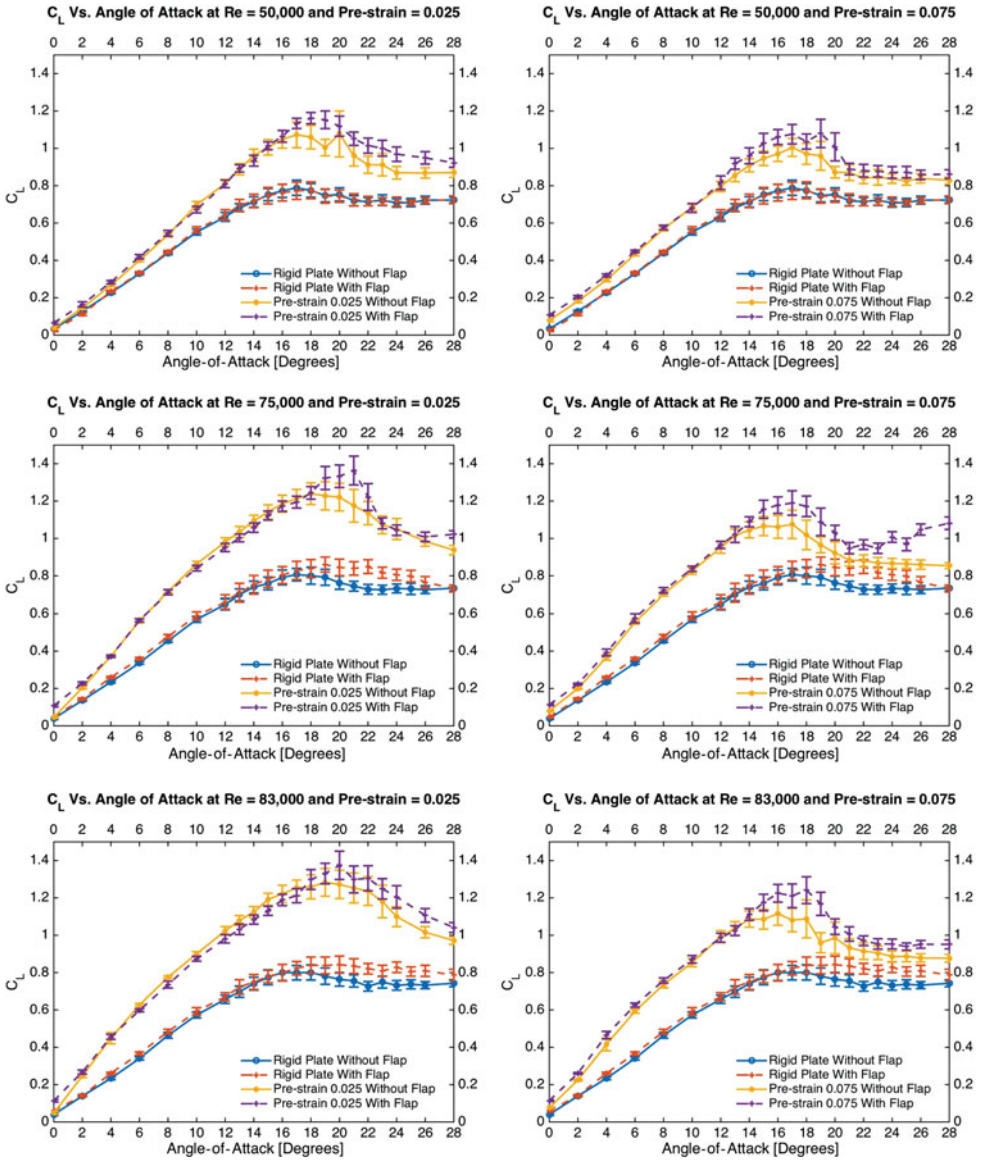

Figure 12. (Colour online) The C_L is plotted against angle-of-attack for pre-strain of 0.025 (left) and pre-strain of 0.075 (right).

Re = 75,000 test condition. The same trends observed in this case are reflected in the other membrane test conditions.

The effect of the flap on C_D is minimal before the stall angle of the clean wing. After this stall angle, there is an increase in C_D that accompanies the increase in C_L. This can be observed in Fig. 15 (left) and Fig. 10, respectively. The behaviour of C_M is also changed with the addition of the flap; in all test conditions where the flap had a measurable effect, the C_M was reduced for low angles of attack and increased for high angles of attack. At first inspection, it may be assumed that the addition of the flap changes the mass distribution of the

https://doi.org/10.1017/aer.2017.10 Published online by Cambridge University Press

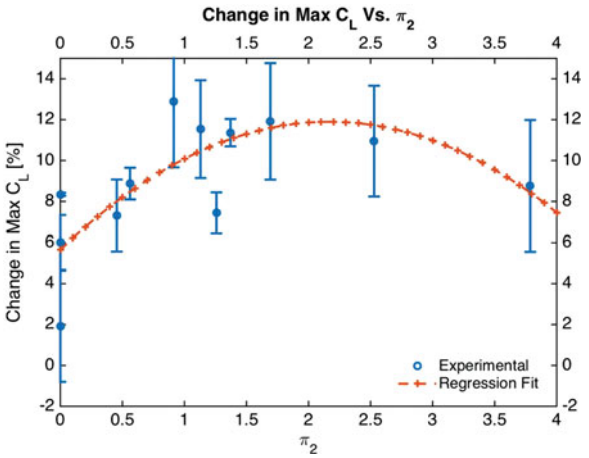

Figure 13. (Colour online) The average increase in maximum lift with the addition of the flap plotted against π_2.

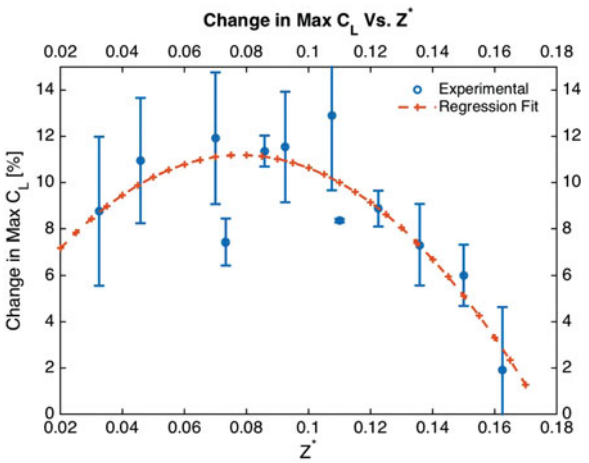

Figure 14. (Colour online) The average increase in maximum lift with the addition of the flap plotted against Z^* of the clean wing[51].

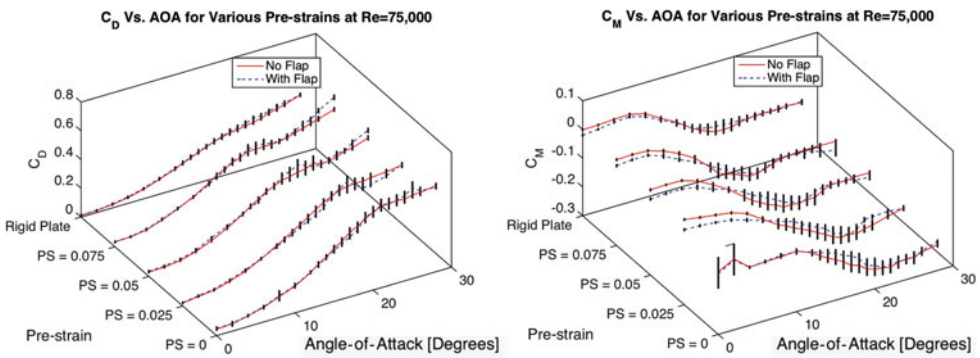

Figure 15. (Colour online) Drag versus angle-of-attack with and without pop-up flap plotted for various pre-strains (left) and pitching moment versus angle-of-attack with and without pop-up flap plotted for various pre-strains (right).

https://doi.org/10.1017/aer.2017.10 Published online by Cambridge University Press

wing and may be responsible for this change in C_M, however, during testing, a new tare file was constructed for each test condition. The independent tare file between the flap and clean conditions means that the observed change is not caused by the mass added by the flap, but rather by an aerodynamic effect of the flap. The observed behaviour of C_M is indicative of a reduction in static stability, and is worthy of further investigation.

6.0 CONCLUSIONS

The effect of a pop-up flap was experimentally measured for three different Re and four levels of pre-strain on an elastic membrane wing as well as on a rigid flat plate. The data collected shows that the Re, pre-strain, and the interaction between the two each have a significant effect on the lift increase caused by the flap. Only the low Re rigid plate and the high Re slack membrane conditions were not found to produce a statistically significant effect on maximum lift. Predicted membrane camber offers the best correlation with lift increase due to the addition of the flap of all metrics evaluated. Relevant findings of this project, specific to the flap configuration tested, include:

- The addition of the pop-up flap increases the maximum lift by 5%-15% for the membrane wing configurations tested; the pop-up flap generates a larger increase in maximum lift for pre-strained membrane wings with respect to a rigid flat-plate.
- Pre-strain, Re, and the interaction term between the two each have a significant effect on the increase in maximum C_L with the addition of the flap. The effect of the interaction term of Re and pre-strain is greater than the effect of pre-strain, which is greater than the effect of Re.
- The effectiveness of the pop-up flap changes with the value of membrane camber. For the flap size, flap position and membrane geometry tested, the flap has a maximum effectiveness when pre-strain is 0.05 and Re is 83,000.

In addition to the primary focus on C_L, results offer additional remarks as follows:

- C_D was consistently observed to increase with the addition of the flap for angles of attack beyond the clean wing stall angle.
- C_M behaviour was consistently observed to change with the addition of the flap. C_M was reduced at low angles of attack and increased at high angles of attack.

ACKNOWLEDGEMENTS

The authors would also like to extend their greatest gratitude to those who have made this research project possible:

- European Office of Aerospace Research & Development (EOARD) of the United States Air Force (USAF) with Dr. Gregg Abate as project monitor
- Aerospace Engineering Department at the Politecnico di Milano University, Italy
- Air Force Office of Scientific Research under DURIP grant FA9550-12-1-0026

REFERENCES

1. Anderson, J. *Inventing Flight: The Wright Brothers & Their Predecessors*, 2004, JHU Press, Baltimore, Maryland, US.
2. Wenham, F. Aerial locomotion and the laws by which heavy bodies impelled through air are sustained, 1st Annual Report of the Aeronautical Society of Great Britain, 1866 http://invention.psychology.msstate.edu/library/Wenham/WenhamLocomotion.html
3. Dimitriadis, G., Gardiner, J., Tickle, P., Codd, J. and Nudds, R. Experimental and numerical study of the flight of geese, *Aeronautical J*, 2015, **119**, (1217), pp 1-30.
4. Manzanera, R. and Smith, H. Flight in nature II: How animal flyers land, *Aeronautical J*, 2015, **119**, (1213), pp 281-299.
5. Hundley, R. and Gritton, E. Future technology-driven revolutions in military operations, Document No. Tech. rep. DB-110-ARPA, 1994, RAND Corporation, DTIC Document.
6. McMichael, J. and Francis, M. Micro air vehicles-toward a new dimension in flight, *DARPA Document*, 1997.
7. Scott, S. and McFarland, C. *Bird Feathers: A Guide to North American Species*, 2010, Stackpole Books, Mechanicsburg, Pennsylvania, US.
8. Brücker, C. and Weidner, C. Separation control via self-adaptive hairy flaplet arrays, Proceedings of the ERCOFTAC International Symposium, Unsteady separation in fluid-structure interaction, June 2013, Mykonos, Greece, pp 17-21.
9. Johnston, J., Gopalarathnam, A. and Edward, J. Experimental investigation of bio-inspired high lift effectors on a 2-D airfoil, 29th AIAA Applied Aerodynamics Conference, number AIAA 2011-3791, 2011, Honolulu, HI.
10. Schatz, M., Bunge, U., Lübcke, H. and Thiele, F. Numerical study of separation control by movable flaps, *Aerodynamic Drag Reduction Technologies*, Notes on Numerical Fluid Mechanics (NNFM), vol 76, 2001, Springer, Berlin, Heidelberg, pp 385-390.
11. Schluter, J. Lift enhancement at low Reynolds numbers using self-activated movable flaps, *J Aircr* 2010, **47**, (1), pp 348-351.
12. Wang, C. and Schluter, J. Low Reynolds' number application of feather inspired passive high lift device on finite wing, 31st AIAA Applied Aerodynamics Conference, 2013, AIAA-2013-2669, San Diego, California, US.
13. Allemand, G. and Altman, A. Post-stall performance improvement through bio-inspired passive covert feathers, 54th AIAA Aerospace Sciences Meeting and Exhibit, 2016, AIAA-2016-2042, San Diego, California, US.
14. Schatz, M., Knacke, T. and Thiele, F. Separation control by self-activated movable flaps, 42th AIAA Aerospace Sciences Meeting & Exhibit, 2004, AIAA-2004-1243, AIAA, Reno, Nevada, US.
15. Bechert, D., Bruse, M., Hage, W. and Meyer, R. Biological surfaces and their technological application – laboratory and flight experiments on drag reduction and separation control, 28th Fluid Dynamics Conference, 1997, Snowmass Village, Colorado, US.
16. Kernstine, K., Moore, C., Cutler, A. and Mittal, R. Initial characterization of self-activated movable flaps, 'Pop-Up Feathers', 46th AIAA Aerospace Sciences Meeting and Exhibit, 2008, Reno, Nevada, US.
17. Traub, L. and Jaybush, L. Experimental Investigation of Separation Control Using Upper-Surface Spoilers, *J of Aircr* 2010, **47**, (2), pp 714-718.
18. G-ograve, Bramesfeld, T. and Maughmer, M. Experimental investigation of self-actuating, upper-surface, high-lift-enhancing effectors, *J of Aircr* 2002, **39**, (1), pp 120-124.
19. Bechert, D., Bruse, M., Hage, W. and Meyer, R. Fluid mechanics of biological surfaces and their technological application, *Naturwissenschaften*, 2000, **87**, (4), pp 157-171.
20. Johnston, J. and Gopalarathnam, A. Investigation of a bio-inspired lift-enhancing effector on a 2D airfoil, *Bioinspiration & Biomimetics*, 2012, **7**, (3) p 036003.
21. Wang, C. and Schlüter, J. Stall control with feathers: Self-activated flaps on finite wings at low Reynolds numbers *Comptes Rendus MeÌącanique*, 2012, **340**, (1), pp 57-66.
22. Dharmadasa, V. Behavior of pop up feathers during flow separation, (2014).
23. Feuvrier, A., Mazellier, N. and Kourta, A. Self-adaptive control of a bluff body wake by means of porous flaps, *Int J Engineering Systems Modelling and Simulation*, 2013, **47**, (5.1-3), pp 57-67.

https://doi.org/10.1017/aer.2017.10 Published online by Cambridge University Press

24. BRÜCKER, C. and WEIDNER, C. Influence of self-adaptive hairy flaps on the stall delay of an airfoil in ramp-up motion, *J Fluids and Structures*, 2014, **47**, pp 31-40.
25. ARIVOLI, D. and SINGH, I. Self-adaptive flaps on low aspect ratio wings at low Reynolds numbers, *Aerospace Science and Technology*, 2016, **59**, pp 78–93.
26. MEYER, R., HAGE, W., BECHERT, D., SCHATZ, M., KNACKE, T. and THIELE, F. Separation control by self-activated movable flaps *AIAA J*, 2007, **45**, (1), pp 191-199.
27. LIU, T., MONTEFORT, J. and PANTULA, S. Effects of flexible fin on low-frequency oscillation in post-stalled flows, *AIAA J*, 2010, **48**, (6), pp 1235-1247.
28. MONTEFORT, J., POHL, N., LIU, T., GREGORY, J. and CRAFTON, J. Thin-wing vibration control using flexible fins, *AIAA J*, 2013, **51**, (9), pp 2218-2230.
29. FAVIER, J., DAUPTAIN, A., BASSO, D. and BOTTARO, A. Passive separation control using a self-adaptive hairy coating, *J Fluid Mechanics*, 2009, **627**, pp 451-483.
30. LENTINK, D., JONGERIUS, S. and BRADSHAW, N. The scalable design of flapping micro-air vehicles inspired by insect flight, *Flying Insects and Robots*, 2009, Springer, Berlin, Heidelberg, pp 185-205.
31. MOHAMED, A., MASSEY, K., WATKINS, S. and CLOTHIER, R. The attitude control of fixed-wing MAVS in turbulent environments, *Progress in Aerospace Sciences*, 2014, **66**, pp 37-48.
32. SMITH, R. and SHYY, W. Computation of aerodynamic coefficients for a flexible membrane airfoil in turbulent flow: A comparison with classical theory, *Physics of Fluids*, 1996, **8**, (12), pp 3346-3353.
33. WALDMAN, R., SONG, A., RISKIN, D., SWARTZ, S., BRUER, K. Aerodynamic behavior of compliant membranes as related to bat flight, 38th AIAA Fluid Dynamics Conference and Exhibit, 2008, Seattle, Washington, US.
34. ROJRATSIRIKUL, P., WANG, Z. and GURSUL, I. Effect of pre-strain and excess length on unsteady fluid-structure interactions of membrane airfoils, *J Fluids and Structures*, 2010, **26**, (3), pp 359-376.
35. GALVAO, R., ISRAELI, E., SONG, A., TIAN, X., BISHOP, K., SWARTZ, S., BREUER, K. The aerodynamics of compliant membrane wings modeled on mammalian flight mechanics, AIAA Paper **2866**, 2006.
36. JAWORSKI, J. and GORDNIER, R. High-order simulations of low Reynolds number membrane airfoils under prescribed motion, *J Fluids and Structures*, 2012, **31**, pp 49-66.
37. PENNYCUICK, C. The Membrane Wings of Bats and Pterosaurs, *Theoretical Ecology Series 5*, chapter 6, 2008, pp 135-160.
38. SONG, A. and BREUER, K. Dynamics of a compliant membrane as related to mammalian flight, Proceedings of the 45th AIAA Aerospace Sciences Meeting and Exhibit, January 2007, Reno, Nevada, US, pp 8-11.
39. ALBERTANI, R., STANFORD, B., HUBNER, J. and IFJU, P. Aerodynamic characterization and deformation measurements of a flexible wing micro air vehicle, *Experimental Mechanics*, 2007, **47**, (4), pp 625-636.
40. GALLIVAN, P. and DELAURIER, J. An experimental study of flapping membrane wings, *Canadian Aeronautics and Space J*, 2007, **53**, (2), pp 35-46.
41. SHYY, W., IFJU, P. and VIIERU, D. Membrane wing-based micro air vehicles, *Applied Mechanics Reviews*, 2005, **58**, (4), pp 283-301.
42. ZHANG, Z., HUBNER, J., TIMPE, A., UKEILEY, L., ABUDARAMV, Y. and IFJU, P. Effect of aspect ratio on flat-plate membrane airfoils, 50th Aerospace Sciences Meeting and Exhibit, *AIAA Paper*. Vol. **1084**, 2012.
43. ABUDARAMV, Y. Wind Tunnel Testing of Load-Alleviating Membrane Wings, Doctoral dissertation, University of Florida, 2009
44. IFJU, P., JENKINS, D., ETTINGER, S., LIAN, Y., SHYY, W. and WASZAK, M. Flexible-wing-based micro air vehicles, *AIAA Paper*. Vol. **705**, 2001 pp 1-11.
45. BABCOCK, J., ALBERTANI, R. and ABATE, G. Experimental estimation of the rotary damping coefficients of a pliant wing, *J Airc*, 2012, **49**, (2), pp 390-397.
46. Modern Machine and Tool Co. Oregon State University Balance OSU-001 Calibration Report, Modern Machine and Tool Documentation, 2012.
47. OSTERBERG, N. Experimental investigation of dynamic stall on pliant wings for micro air vehicles, 54th AIAA Aerospace Sciences Meeting, 2016, AIAA-2016-0146, San Diego, California, US.
48. CARPENTER, T. and ALBERTANI, R. Aerodynamic load estimation from virtual strain sensors for a pliant membrane wing, *AIAA J*, **53.8**, (2015), pp 2069-2079.

https://doi.org/10.1017/aer.2017.10 Published online by Cambridge University Press

49. Stanford, B. Fixed membrane wings for micro air vehicles: Experimental characterization, numerical modeling, and tailoring, *Progress in Aerospace Sciences*, 2008, **44**, (4), pp 258-294.
50. Zhang, Z., Hopper, L., Wrist, A., Hubner, J. and Ukeiley, L. Nondimensional frequency scaling of aerodynamically-tensioned membranes, *J Fluids and Structures*, 2014, **48**, pp 14-26.
51. Waldman, R. and Breuer, K. Shape, lift, and vibrations of highly compliant membrane wings, 43rd Fluid Dynamics Conference, 2013, AIAA, Reston, Virginia, US, pp 1-20.
52. Song, A., Tian, X., Israeli, E., Galvao, R., Bishop, K., Swartz, S. and Breuer, K. Aeromechanics of membrane wings with implications for animal flight, *AIAA J*, 2008, **46**, (8), pp 2096-2106.
53. Waszak, M., Jenkins, L. and Ifju, P. Stability and control properties of an aeroelastic fixed wing micro aerial vehicle, AIAA Paper **4005**, 2001.
54. Rojratsirikul, P., Genc, M., Wang, Z. and Gursul, I. Flow-induced vibrations of low aspect ratio rectangular membrane wings, *J Fluids and Structures*, 2011, **27**, (8), pp 1296-1309.
55. Ramsey, F. and Schafer, D. *The Statistical Sleuth: A Course in Methods of Data Analysis*, 2013, Cengage Learning, Boston, Massachusetts, US.
56. Montgomery, D. *Design and Analysis of Experiments*, 2013, John Wiley & Sons, Hoboken, New Jersey, US.

https://doi.org/10.1017/aer.2017.10 Published online by Cambridge University Press